

https://doi.org/10.1070/QEL16379

Study of the formation of thermochemical laser-induced periodic surface structures on Cr, Ti, Ni and NiCr films under femtosecond irradiation*

A.V. Dostovalov, V.P. Korolkov, V.S. Terentyev, K.A. Okotrub, F.N. Dultsev, S.A. Babin

Abstract. **The formation of femtosecond laser-induced periodic surface structures (LIPSS's) on Cr, Ti, Ni and NiCr films (with different Cr contents) is investigated. It is established that thermochemical LIPSS's with periods of 950, 930 and 980 nm are formed, respectively, on the surfaces of titanium, chromium, and nichrome (with a chromium content of 20%); however, thermochemical LIPSS's are not formed on the surfaces of nickel and nichrome with a low chromium content, although Raman data indicate that oxidation occurs in all cases. A weakly ordered ablated structure with a period of 250–300 nm is found to be formed on oxidised areas of thermochemical LIPSS's in the case of chromium and nichrome (80/20). Experimental data on selective etching of thermochemical LIPSS's on titanium and chromium films are presented.**

Keywords: *thermochemical laser-induced periodic surface structures, femtosecond laser nanostructuring, laser thermochemistry, ablation, Raman scattering, selective etching.*

1. Introduction

Since the beginning of the 1960s, when lasers were invented, the effects of laser irradiation on various materials, including metals, have been intensively studied. Along with applied problems (laser cutting of metals, welding, and drilling holes), these studies were aimed to gain insight into the nature of the physical processes occurring under laser irradiation. When studying ablation (removal of material from the surface), metals were found to form laser-induced periodic surface structures (LIPSS's) in the area of a focused laser spot, having a period somewhat smaller than the radiation wavelength and oriented perpendicularly to the incident beam polarisation direction (Figs 1a–1c) [1]. Here, the irradiated area size greatly exceeds the structure period, and focusing is generally used to obtain a necessary energy density. The generally accepted theory [2] explaining the LIPSS formation is based on the interference between the incident radiation and surface electromagnetic waves, which are generated on resonance periodic gratings existing in the spatial spectrum of random irregularities of a metal surface. As a result of this interference, the intensity becomes periodically modulated on the surface. In the modulation maxima, when the intensity exceeds a certain threshold value, the material is ablated, and a surface profile is formed (see Fig. 1d). Many studies have been devoted to the structures of this type formed on different materials (metals, insulators and semiconductors), due to which the formation of ablation LIPSS's has been investigated in detail to date [3].

A relatively short time ago, it was demonstrated that femtosecond laser irradiation of a titanium film leads to the formation of new-type (thermochemical) LIPSS's on its surface [4, 5]. They are formed due to metal oxidation rather than as a result of ablation; therefore, a rise in the relief height is observed in this case (Fig. 1g). Other specific features of the structures of this type, as compared with ablation LIPSS's, are as follows: high degree of order, absence of phase shifts and orientation parallel to the incident beam polarisation direction (Figs 1a, 1e and 1f).

Since the first results on the formation of thermochemical LIPSS's (TLIPSS's) were obtained on titanium films, it is important to investigate the possibility of forming such structures on the surface of films of other metals and alloys.

In this paper, we report the experimental results on the formation of TLIPSS's on the surface of Cr, Ni and NiCr films (with different Cr contents) in comparison with the data on titanium films. These metals were chosen in view of their wide use in the microelectronic industry and the existence of etching technologies for different-purpose microstructures in them. It is noteworthy that some known technologies of forming microstructures on metal films are based on the masking properties of their oxides [6]. In this context, it is important to determine the possibility of using TLIPSS's as masks for selective etching of a metal film on which they are formed.

2. Experimental

The studies were performed on a laser micromachining system consisting of a PHAROS 6W femtosecond laser (Light Conversion Ltd), having a fundamental harmonic wavelength of 1026 nm, pulse width of 232 fs, pulse energy of 70–102 nJ and pulse repetition rate of 200 kHz, and a high-precision Aerotech ABL1000 stage. The sample displacement velocity in the experiments was 3.5 μm s^{-1}. To monitor the writing pro-

* Presented at the Fundamentals of Laser Assisted Micro- and Nanotechnologies (FLAMN-16) International Symposium (Pushkin, Leningrad oblast, 27 June to 1 July 2016).

A.V. Dostovalov, V.P. Korolkov, S.A. Babin Institute of Automation and Electrometry, Siberian Branch, Russian Academy of Sciences, prosp. Akad. Koptyuga 1, 630090 Novosibirsk, Russia; Novosibirsk State University, ul. Pirogova 2, 630090 Novosibirsk, Russia; e-mail: dostovalov@iae.nsk.su;
V.S. Terentyev, K.A. Okotrub Institute of Automation and Electrometry, Siberian Branch, Russian Academy of Sciences, prosp. Akad. Koptyuga 1, 630090 Novosibirsk, Russia;
F.N. Dultsev A.V. Rzhanov Institute of Semiconductor Physics, Siberian Branch, Russian Academy of Sciences, prosp. Akad. Lavrent'eva 13, 630090 Novosibirsk, Russia

Received 24 March 2017
Kvantovaya Elektronika **47** (7) 631–637 (2017)
Translated by Yu.P. Sin'kov

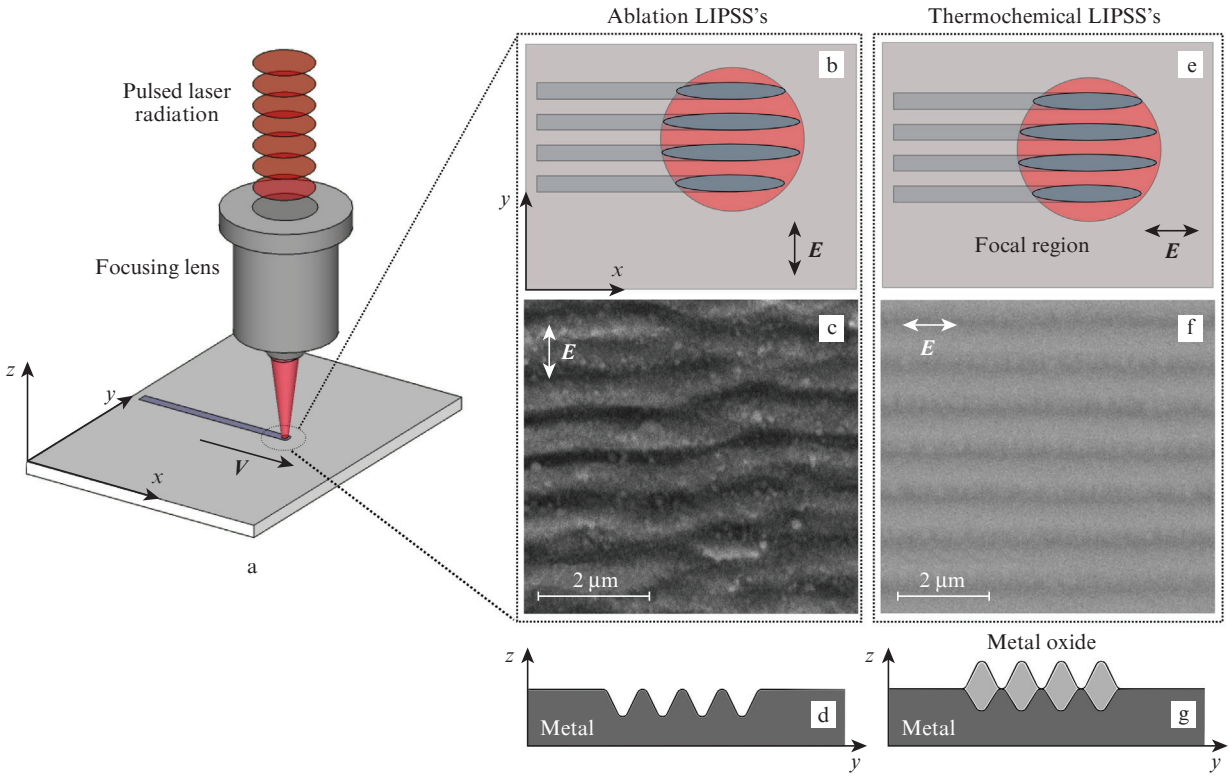

Figure 1. Specific features of the formation of ablation and thermochemical LIPSS's on metals.

cess and provide exact positioning of the exposed area on the sample surface, we used a digital camera and a LED system illumination. The focused-beam diameter was $2w_0 = 14.7$ μm. The nanostructures formed on the sample surface were investigated with a Hitachi TM3000 scanning electron microscope (SEM) and an Integra atomic-force microscope (AFM). Metal films were deposited on a fused silica substrate by magnetron sputtering in argon. The film thickness was in the range of 400–600 nm. The chemical composition of the films was investigated using Raman spectroscopy. The excitation radiation source was a solid-state Millennia II laser (Spectra Physics) with a wavelength of 532.1 nm. The experiment was performed in the backscattering regime; a microscopic objective with NA = 0.75 was used to focus the excitation beam and collect scattered light. Raman spectra were registered from an area of ~1.2 μm^2 in size. The scattered light spectrum was measured by an SP-2500i monochromator (Princeton Instruments), equipped with a multichannel Spec-10:256E/LN CCD detector (Princeton Instruments). The wavelengths of measured spectra were calibrated using the emission spectrum of a neon lamp.

3. Results

In the case of titanium film samples, one can observe the formation of highly ordered TLIPSS's (directed along the polarisation vector of the incident beam) with a period of ~950 nm, which is somewhat smaller than the excitation radiation wavelength (1026 nm) (Fig. 2a). The structures reach 160 nm in height (Fig. 2b). More details of the TLIPSS formation on titanium films can be found in [7].

For the chromium film (Fig. 3), along with the TLIPSS's having a period of 930 nm, one observes the formation of ablated structures with a period of 250–300 nm, oriented

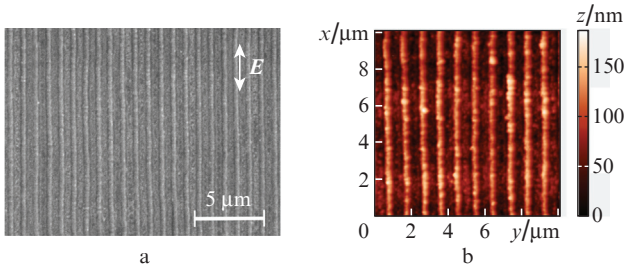

Figure 2. (a) SEM image of the TLIPSS's formed on a titanium surface by laser radiation with energy $W = 71$ nJ and (b) the corresponding AFM image.

perpendicular to the incident beam polarisation direction. The height of the oxide structures is about 100 nm, while the depth of the ablation structures is 50–100 nm. There are oxide nanoparticles on some areas of the structure surface, which can be seen as bright spots in both SEM and AFM images (Figs 3a and 3b). The relief height on these areas reaches 250–300 nm. It is of interest that the nanoparticles, which were apparently formed as a result of the redeposition of the oxide removed during ablation, are concentrated mainly on the grating protrusions. With an increase in the pulse energy, the nanoparticles are significantly reduced in size and begin to be concentrated mainly on the barriers around TLIPSS's (Figs 3c and 3d), which were absent at lower energies.

In the case of NiCr samples (80/20) with a Cr content of 20%, one can observe the formation of structures with a period of 980 nm, oriented parallel to the beam polarisation direction. As in the case of chromium films, ablated structures with a period of 250–300 nm, oriented perpendicular to the beam polarisation direction, are also formed (Fig. 4).

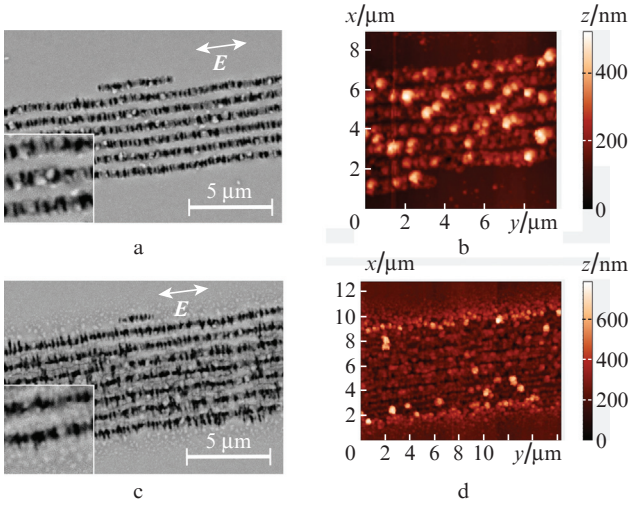

Figure 3. (a, c) SEM images of the TLIPSS's formed on a chromium surface by laser radiation with W = (a) 83 and (c) 102 nJ and (b, d) the corresponding AFM images. The insets in panels (a) and (c) show enlarged images of the structure.

In contrast to the TLIPSS's formed on chromium film, the ablation of NiCr samples leads to the through removal of oxide and, possibly, removal of metal in the central part of the TLIPSS protrusions to a depth up to 300 nm (Figs 4b and 4d).

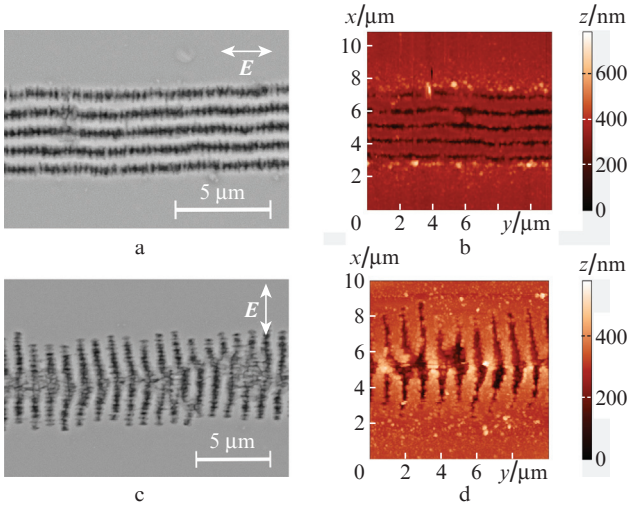

Figure 4. (a, c) SEM images of the TLIPSS's formed on a nichrome (80/20) surface by laser radiation with W = 83 nJ and beam polarisation oriented (a) parallel and (c) perpendicular to the scanning direction and (b, d) the corresponding AFM images.

TLIPSS's are absent of the surfaces of the NiCr sample (94/6) with a lower Cr content (6%) and the pure Ni sample; one can observe only ablation (Fig. 5), which does not lead to the formation of surface periodic structures. It is noteworthy that the anomalously high tendency to oxidation, which is typical of the NiCr (94/6) alloy under steady-state conditions of thermochemical oxidation [8], does not manifest itself under femtosecond laser irradiation. At the same time, this impact causes the formation of oxide periodic structures on

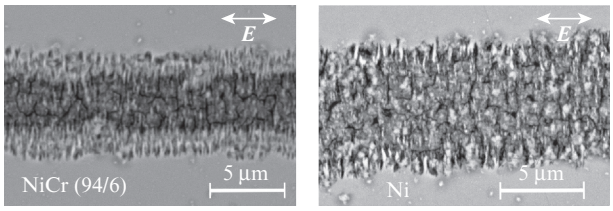

Figure 5. SEM images of the TLIPSS's formed (a) on the nichrome (94/6) surface by laser radiation with W = 75 nJ and (b) on the nickel surface by radiation with W = 79 nJ.

films of standard nichrome NiCr (80/20), which is poorly oxidised under steady-state conditions.

4. Raman spectroscopy study of the chemical composition

The chemical composition of the TLIPSS samples was analysed using Raman spectroscopy. Figure 6 shows the measured Raman spectra of the TLIPSS's formed on titanium, chromium, nickel and nichrome (80/20) films.

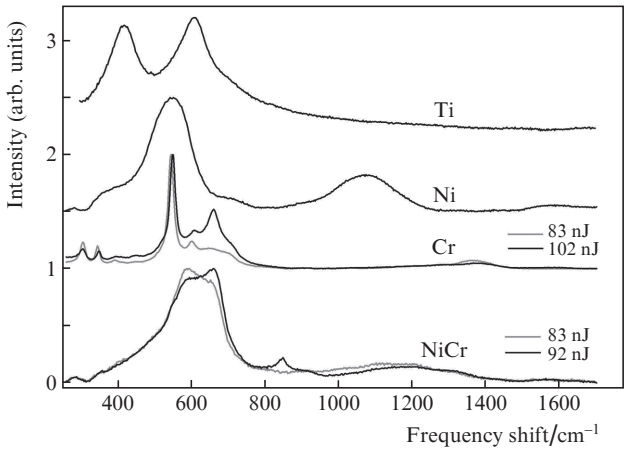

Figure 6. Raman spectra of the TLIPSS's formed on Ti, Ni, Cr and NiCr films. For clarity, the spectra are shifted in the vertical direction.

The Raman spectrum of the TLIPSS's formed on a titanium film contains two peaks at frequencies ν = 418 and 607 cm^{-1}, which correspond to the Raman peaks of rutile (one of the phases of crystalline TiO_2). The peak at ν = 607 cm^{-1} is shifted with respect to the similar Raman peak of rutile single crystal ($\nu = 612 \pm 3$ cm^{-1} [9]). This red shift may be due to the small crystallite size; in this case, a shift by 5 ± 2 cm^{-1} should correspond to a rutile crystallite size of ~10 nm [10]. In the case of single crystal, the peak at ν = 418 cm^{-1} should be at $\nu \approx 447$ cm^{-1} [9]. Thus, the peak in the recorded spectra is shifted by almost 30 cm^{-1}. This shift can also be partly explained by the size effect; however, the corresponding shift for the aforementioned peak should not exceed 3 cm^{-1} [10]. Another possible reason for this large shift is the oxidation nonstoichiometry. According to the data of [11], the ratio of the oxygen and titanium concentrations ([O]/[Ti]) in the structures formed should not exceed 1.9, even taking into account the additional shift caused by the size effect.

The Raman spectrum of the structures formed on the nickel film contains peaks at $\nu = 547$ and 1072 cm^{-1} (overtone) and a weak band at $\nu \approx 1580$ cm^{-1}, which is due to the scattering from magnons (Fig. 6). The peak positions in the Raman spectrum are close to the positions of the lines of single-crystal nickel oxide NiO at $\nu = 560$, 1100, and 1600 cm^{-1} [12]. The discrepancy (red shift) of the positions may be due to the small crystallite size. The nickel oxide line was observed at $\nu \approx 556$ cm^{-1} for 100-nm crystallites in [13]; the small crystallite size is also evidenced by the low peak intensity at $\nu \approx 1580$ cm^{-1}.

Raman spectra of the TLIPSS's formed on a chromium film were obtained for two laser pulse energies W (Fig. 6). The Raman spectrum recorded at $W = 83$ nJ contains lines at $\nu = 306$, 346, 393, 446, 545 and 602 cm^{-1}, which correspond to the Cr_2O_3 phase [14]. At $W = 102$ nJ, the peak positions somewhat change: $\nu = 305$, 349, 397, 450, 550 and 608 cm^{-1}. A new peak arises at $\nu = 660$ cm^{-1}, which indicates the presence of chromium oxide CrO_2.

The Raman spectrum of the TLIPSSs formed on a nichrome (80/20) film is similar to that of nickel oxide. A combined band at $\nu \approx 620$ cm^{-1} and its overtone at $\nu = 1150-1200$ cm^{-1} are observed. An increase in the pulse energy leads to the occurrence of a CrO_2 peak at $\nu = 660$ cm^{-1} and a line at $\nu = 849$ cm^{-1}, which corresponds to nichrome oxide [15].

5. Discussion of the experiments on the TLIPSS formation

As the experimental results showed, TLIPSS's are formed on only some of metals and alloys. The difference in the behaviour of metal films may be related to the difference in the three types of the material characteristics and/or their combinations: the thermophysical parameters, the change in the fraction of absorbed laser energy during surface irradiation due to the formation of an oxide film and a surface relief grating, the activation energy and the oxidation reaction rate. Table 1 contains some physical characteristics of the metals under study and their oxides. Nickel has higher thermal and electrical conductivities than Cr and Ti, which should lead to a more rapid smoothing of the periodic spatial modulation of the electron temperature on the metal surface, remaining after the exposure to the beam interfering with surface defects. Among the metals under consideration, titanium has the lowest thermal conductivity, which provides the highest order of the TLIPSS's formed on its surface.

From the point of view of radiation energy absorption during the oxide layer growth, an increase in the oxide thickness should lead (for all three metals) to a periodic change in the absorption by a factor of about 2–2.5 due to the interference. In the initial stage of oxide formation, absorption increases and reaches a maximum at a thickness of 70–120 nm, depending on the refractive index. Thus, concerning the optical properties, all the metals under study should behave similarly.

Let us consider the thermochemical aspect of the formation of oxide periodic surface structures. When studying the oxidation of metals, two mechanisms of the formation and growth of an oxide film are selected: (i) the diffusion of metal cations and electrons through the oxide layer to the oxide surface with subsequent interaction with oxygen and formation of an oxide film at the gas--oxide interface and (ii) the diffusion of oxygen anions through the oxide layer to the metal surface and subsequent interaction with the metal, accompanied by the formation of an oxide film at the metal–oxide interface. A limiting factor for the chemical reaction is the slowest process. The theoretical description of the metal oxidation differs in dependence of the thickness of the oxide film formed during the chemical reaction. Thin films are described well within the Cabrera–Mott theory [16], which considers the ion transport through an oxide metal in the presence of an electric field, induced by the transition of electrons through the thin oxide layer (either due to the tunnel effect or because of the thermionic emission). In this case, the oxide film growth is described by the expression

$$\ln(\mathrm{d}l/\mathrm{d}t) = B_1 + B_2/l,$$

where l is the oxide-layer thickness; t is the oxidation reaction time; and B_1 and B_2 are constants. As was indicated in [17], this theory can be applied to oxide thicknesses on the order of 10 nm. It was also found in [17] that the films with thicknesses exceeding the Debye screening length (which amounts to 0.1–1 μm) can be described within the Wagner theory, in which the limiting process is the ion diffusion through the oxide film; the influence of the electric field in the oxide is disregarded. The oxide film growth in the latter case is described by a parabolic law [18]:

$$\frac{\mathrm{d}l}{\mathrm{d}t} = \frac{\varkappa(T)}{l}, \quad \varkappa(T) = \varkappa_0 \exp\left(-\frac{Q}{RT}\right),$$

where $\varkappa(T)$ is the parabolic oxidation rate constant and Q is the activation energy of the oxidation reaction.

In this study, the measured height of the structures above the metal surface is ~160 nm (for titanium); in addition, there is an oxide film of certain thickness under the metal surface. Therefore, the total oxide-layer thickness is ~200–300 nm; i.e., it falls in the range of thicknesses where none of the two

Table 1. Physical characteristics of metals and their oxides.

Element	Melting temperature (°C)	Thermal conductivity/ W m^{-1} K^{-1}	Density/ g cm^{-3}	Specific heat/ J kg^{-1} K^{-1}	Electrical conductivity/ Ω^{-1} m^{-1}	Optical constants n and k for $\lambda = 1030$ nm
Ti	1665	22	4.5	544	2.4×10^6	3.35; 3.3
TiO_2	1843	12	4.2	–	–	2.75; 0
Cr	1907	67	7.2	460.5	8×10^6	3.5; 3.58
Cr_2O_3	2435	10	5.2	–	–	2.2; 0
Ni	1455	91	8.9	502.4	1.4×10^7	2.85; 5.1
NiO	1955	5	6.7	–	–	2.3; 0.028
NiCr (80/20)	1400	12	8.4	460.5	8.3×10^5	–
NiCr (90/10)	–	17	8.6	–	–	–

theories describe adequately the oxidation kinetics. Nevertheless, the thickness of the TLIPSS oxide layer is formally closer (on the order of magnitude) to the thickness range for which the Wagner theory is valid. It was suggested in [19] that the Wagner theory can be applied to the case of oxidation of thin chromium films by femtosecond laser radiation, although, in contrast to our experiments, pulses with a repetition rate of 80 MHz were used in that study.

Table 2 contains the parabolic oxidation rate constants at a temperature of $T = 1000\,^{\circ}\mathrm{C}$ for the metals under consideration. This parameter is much larger for titanium than for nickel and chromium; therefore, the oxidation reaction and formation of TLIPSS's should be most efficient in this case. As was noted above, the periodic spatial modulation of the electron temperature on the metal surface is smoothed more rapidly in the case of nickel; therefore, despite the growth of an oxide film, whose presence was evidenced by the Raman spectra, its thickness modulation is insufficient for the formation of a stable highly ordered periodic grating, and the uniform thermochemical oxidation is transformed into the ablation regime.

Table 2. Parabolic oxidation rate constants.

Ion	Oxide	$\varkappa/\mathrm{cm}^2\,\mathrm{s}^{-1}$ at $T = 1000\,^{\circ}\mathrm{C}$	References
Ti	TiO_2	5.8×10^{-10}	[20]
Cr	Cr_2O_3	3.2×10^{-11}	[21]
Ni	NiO	3.4×10^{-11}	[22]

The formation of ablated structures with periods of 250–300 nm, which are shown in Figs 3 and 4, is likely caused by the well-known effect of the formation of ablation LIPSS's on a metal surface under a layer of insulator or liquid, in which (according to [23]) the structure period is $\Lambda = \lambda/\mathrm{Re}\eta$, where λ is the radiation wavelength (1026 nm), $\eta = \sqrt{\varepsilon_d\varepsilon_m/(\varepsilon_d + \varepsilon_m)}$, ε_d is the insulator permittivity, $\varepsilon_m = \varepsilon'_m + i\varepsilon''_m$ is the complex permittivity of the metal, $\varepsilon'_m = n^2 - k^2$ and $\varepsilon''_m = 2nk$. In our case, after the formation of an oxide layer (transparent for incident light), subsequent laser pulses are absorbed at the metal–oxide interface, where surface electromagnetic waves are induced, and, according to the mechanism described in the Introduction, ablation LIPSS's are formed in the metal oxide; these structures are oriented perpendicular to the incident beam polarisation direction. With allowance for the data in Table 1 for the chromium oxide refractive index, the period can be estimated as ~300–400 nm, values close to the experimental results. The observed LIPSS periods are in agreement with the data of other studies devoted to the femtosecond laser processing of metal oxides [24, 25], where $\Lambda \approx \lambda/4$ for oxides of different metals. In the case of nichrome, chromium is the first to be oxidised; therefore, the period of ablation LIPSS is also close to the value found for chromium.

6. Selective etching of metals through a mask of their oxides

If the topology of TLIPSS's is transferred to the metal sublayer on which they were formed, new promising fields of their application may arise, including the technologies of micromechanical devices and microsensors. The transfer can be performed using selective plasma or liquid etching of metals through the oxide grating mask. These approaches are based on the known data on selective liquid and plasma etching of metals through masks of their oxides [6, 26].

A known thermochemical technology of designing the topology of photomasks on chromium films (30–100 nm) deposited on a glass substrate implies their local heating by a focused cw [27] or pulsed [26] laser beam and the formation of a chromium oxide mask with a thickness of about 5–10 nm. After the laser recording, the photomask pattern is developed by liquid etching in a solution containing six parts of 25% $K_3Fe(CN)_6$ aqueous solution and one part of 25% NaOH aqueous solution. Typical etching times range from 3 to 5 min.

By analogy with this technology, we investigated the possibility of selective liquid etching of the TLIPSS's formed on a 300-nm-thick chromium film, using the same etchant. The structures arose at laser pulse energies from 37 to 63.5 nJ and focal spot diameter of 8.5 μm. The micrographs of the structures, recorded in reflection using a Zeiss AxioImager optical microscope with an objective $100^{\times}$, are shown in Fig. 7. In the first stage, etching was performed for 1 min in a standard photolithography etchant of chromium (based on cerium sulphate), which is much less selective to chromium oxide than the aforementioned solution. This stage is necessary to remove the thin oxide film, which also grows between grating protrusions. Then we carried out a long-term etching in the second etchant, based on $K_3Fe(CN)_6$ and NaOH. Breaks in etching were made to record relief micrographs using the Zeiss AxioImager optical microscope equipped with an $100^{\times}$ objective.

At a laser pulse energy of 37 nJ, periodic structures did not arise; instead, only a wide track of a thin oxide layer (hardly visible in an optical microscope) was formed on the surface. During etching, it became visible well (Fig. 7b). It can be seen that the TLIPSS region is surrounded by a contour with a width of about 3 μm, which arises due to conventional thermochemical process under the action of spreading heat. This contour is etched away for 15 min, simultaneously with the wide oxide track formed at a laser pulse energy of 37 nJ. The unprocessed part of the chromium film is etched away by the 11th minute. At the same time, TLIPSS's are not etched away, at least by the 32th minute (Fig. 7c). This means that, because of the interference energy redistribution, the metal film undergoes deep oxidation. The SEM image indicates that, at laser pulse energies of 45–57 nJ, the grating lines with a period less than 1 μm are clearly separated. The inset in Fig. 7c shows the chromium concentration distribution over the structure. It can be seen that the grooves contain neither chromium nor its compounds. The formation of this structure on a chromium film with a thickness of several hundreds of nano-

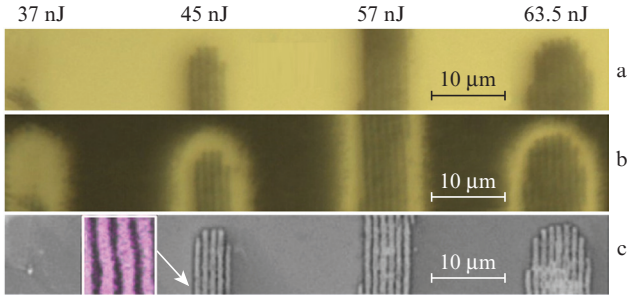

Figure 7. (a, b) Optical images of TLIPSS's (a) before etching and (b) after 7-min etching in the second etchant and (c) a SEM image after 32-min etching in the second etchant.

metres by photolithography (liquid etching through a photoresist mask) would be difficult due to the isotropic character of metal film etching.

7. Titanium etching in inductively coupled plasma

Parker et al. [6] described the formation of deep structures with a high aspect ratio in bulk titanium samples and foils by etching through a TiO_2 mask, formed by photolithography on a deposited 1.25-μm-thick titanium oxide film using a photoresist mask and etching in CHF_3 inductively coupled plasma (ICP). Then the topology was transferred on the titanium surface by ICP etching in a mixture of Cl_2 (100 cm^3 min^{-1}) and Ar (5 cm^3 min^{-1}). The selectivity of Ti etching with respect to TiO_2 reached 40:1 at an etch rate of 2 μm min^{-1}. Under these conditions, the microelements had a form of walls with a height of 20 μm and a width of 1 μm. For the TLIPSS's formed on thin (below 400 nm) titanium films, the typical height of oxide tracks is within 100–150 nm at a period of ~950 nm. According to the data of [5], these tracks are porous and rounded.

Reactive ion etching of TLIPSS's on titanium films was performed using the Plasmalab 100Plus system in the ICP regime. A mixture of chlorine-containing gas with Ar (CCl_2F_2 + Ar or Cl_2 + Ar) with a feed rate of 20 cm^3 min^{-1} was used. The RF discharge and ICP powers were, respectively, 100 and 400 W. The pressure in the camera was 15 mTorr. The etching was carried out in 1-min steps, with 1-min cooling after each step. The result of 5-min TLIPSS etching is shown in Fig. 8a. The etching led to the formation of a high-quality grating, with a depth reaching the glass. Further etching for five more minutes led to exfoliation of the structure (Fig. 8b), which was most likely caused by the undercutting etching and mechanical stress.

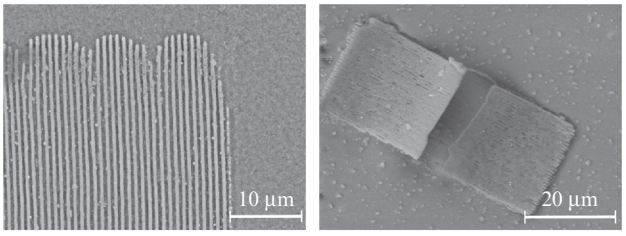

Figure 8. SEM images of the structures obtained by selective reactive ion etching [(a) for 5 min and (b) for 10 min] of the TLIPSS's formed on the titanium film surface.

To determine the profile of etched grating protrusions, a titanium film was deposited on a silicon wafer. After the formation of a TLIPSS grating on it, the plate was cleaved across the periodic structure (SEM image in Fig. 9a). The top view of the TLIPSS grating, recorded with the SEM, is shown in Fig. 9b. The micrograph of the cleavage indicates that the oxide layer thickness under the initial surface of the metal film is twice as large as that above the surface. Figures 9c and 9d show also a wafer cleavage made across the periodic structure and the top view of the structure after the ICP etching. The slope of the grating protrusion walls is due to the smooth decrease in the thickness of the oxide tracks visible in Fig. 9a.

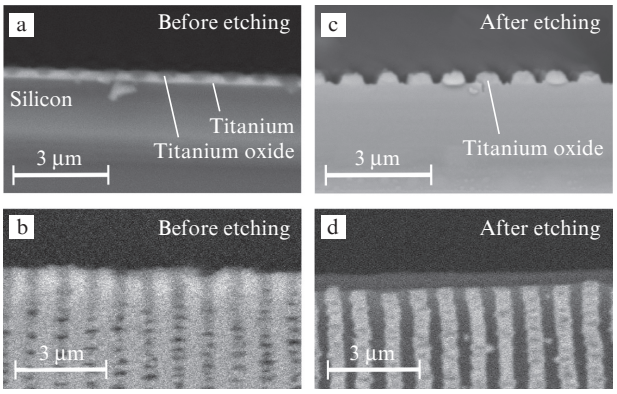

Figure 9. SEM images of the TLIPSS's formed on a titanium film deposited on a silicon substrate: the structures before etching: (a) cleavage and (b) a top view and (c, d) the corresponding images after etching.

8. Conclusions

The experiments on the formation of LIPSS's on Cr, Ti, Ni and NiCr (with different Cr contents) films showed that TLIPSS's with periods of 950, 930 and 980 nm arise on the surface of titanium, chromium and nichrome (with an chromium content of 20%) films, respectively. At the same time, TLIPSS's are not formed on the surface of films of nickel and nichrome with a low chromium content, because nickel has a higher thermal conductivity than Cr and Ti, which leads to smoothing the periodic spatial modulation of electron temperature. The formation of a weakly ordered ablated structure with a period of 250–300 nm on the oxidised TLIPSS portions was revealed in the case of chromium and nichrome (80/20) films; this pattern is explained by the formation of ablation LIPSS's on the metal–oxide interface.

The Raman study of the TLIPSS chemical composition showed the presence of oxides of the corresponding metals for each sample, as well as the presence of nanocrystallites in the oxide structure.

Along with the specific features of the formation of TLIPSS's, we considered the problems related to their selective etching. Our study confirmed that the TLIPSS's formed on chromium films can be transported to the metal sublayer by a two-stage liquid etching, using an etchant based on cerium sulphate and ammonium in the first stage and a selective etchant based on potassium ferricyanide in the second stage. The TLIPSS's formed on titanium films can be etched through to the substrate surface, using reactive ion ICP etching in a chlorine-containing gas. These results may condition the occurrence of new practical applications of laser-induced periodic structures.

Acknowledgements. We are grateful to A.S. Kozlov for the AFM measurements and to S.L. Mikerin and A.E. Simanchuk for the SEM measurements.

This work was supported by the Russian Foundation for Basic Research (Grant No. 16-32-60096). V.P. Korolkov acknowledges the support of the Russian Foundation for Basic Research (Grant No. 14-29-07227). The experiments were carried out at the Centre for Collective Use of Scientific Equipment 'High-Resolution Spectroscopy of Gases and Condensed Media' at the Institute of Automation and Electrometry of the Russian Academy of Sciences (Siberian Branch).

References

1. Isenor N.R. *Appl. Phys. Lett.*, **31**, 148 (1977).
2. Bonch-Bruevich A.M., Libenson M.N., Makin V.S. *Usp. Fiz. Nauk*, **155**, 2 (1988).
3. Vorobyev A.Y., Guo C. *Laser Photonics Rev.*, **7**, 385 (2012).
4. Öktem B., Pavlov I., Ilday S., Kalaycıoğlu H., Rybak A., Yavaş S., Ilday F.Ö. *Nat. Photonics*, **7**, 897 (2013).
5. Dostovalov A.V., Korolkov V.P., Babin S.A. *Laser Phys. Lett.*, **12**, 036101 (2015).
6. Parker E.R., Thibeault B.J., Aimi M.F., Rao M.P., MacDonald N.C. *J. Electrochem. Soc.*, **152**, 675 (2005).
7. Dostovalov A.V., Korolkov V.P., Babin S.A. *Appl. Phys. B*, **123**, 30 (2017).
8. Kofstad P. *High-Temperature Oxidation of Metals* (New York: Wiley, 1966; Moscow: Mir, 1969).
9. Parker J.C., Siegel R.W. *J. Mater. Res.*, **5**, 1246 (1990).
10. Swamy V., Muddle B.C., Dai Q. *Appl. Phys. Lett.*, **89**, 1 (2006).
11. Parker J.C., Siegel R.W. *Appl. Phys. Lett.*, **57**, 943 (1990).
12. Mironova-Ulmane N., Kuzmin A., Sildos I., Pärs M. *Cent. Eur. J. Phys.*, **9**, 1096 (2011).
13. Mironova-Ulmane N., Kuzmin A., Steins I., Grabis J., Sildos I., Pärs M. *J. Phys.: Conf. Ser.*, **93**, 012039 (2007).
14. Mougin J., Rosman N., Lucazeau G., Galerie A. *J. Raman Spectrosc.*, **32**, 739 (2001).
15. Sureshkannan G., Velliangiri M. *Int. J. Mech. Eng. Rob. Res.*, **2**, 265 (2013).
16. Cabrera N., Mott N.F. *Rep. Prog. Phys.*, **12**, 163 (2002).
17. Bailey J.M., Ritchie I.M. *Oxid. Met.*, **30**, 405 (1988).
18. Bunkin F.V., Kirichenko N.A., Luk'yanchuk V.S. *Usp. Fiz. Nauk*, **138**, 45 (1982).
19. Dyukin R.V., Martsinovskiy G.A., Sergaeva O.N., Shandybina G.D., Svirina V.V., Yakovlev E.B. *Interaction of Femtosecond Laser Pulses with Solids: Electron/Phonon/Plasmon Dynamics* (Croatia: InTech, 2012) p. 197.
20. Rodionov I.V. *Doct. Diss.* (Saratov State Technical University, Saratov, 2011).
21. Taneichi K., Narushima T., Iguchi Y., Ouchi C. *Mater. Trans.*, **47**, 2540 (2006).
22. Gulbransen E.A., Andrew K.F. *J. Electrochem. Soc.*, **101**, 128 (1954).
23. Bonch-Bruevich A.M. *Opt. Eng.*, **31**, 718 (1992).
24. Gottmann J., Wortmann D., Wagner R. *Proc. SPIE*, **7022**, 702202 (2007).
25. Shinonaga T., Tsukamoto M., Horigutchi N., Ito Y., Nagai A., Yamashita K., Hanawa T., Matsushita N., Guoqiang X., Takahashi M., Abe N. *Proc. Conf. ICALEO* (Tokyo, Japan, 2012) Vol. 41, p. 25.
26. Veiko V.P., Jarchuk M.V., Ivanov A.I. *Laser Phys.*, **22**, 1310 (2012).
27. Cherkashin V.V., Churin E.G., Burge J.H., Koronkevich V.P., et al. *Proc. SPIE*, **3010**, 168 (1997).